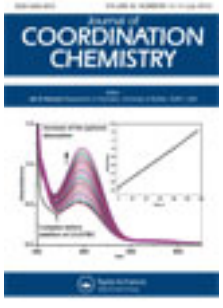

Journal of Coordination Chemistry
Publication details, including instructions for authors and subscription information:
http://www.tandfonline.com/loi/gcoo20

Preparation of $BaCrO_4$ particles in the presence of EDTA from aqueous solutions

Xue-Song Liang [a] , Jia-Hu Ouyang [a] & Zhan-Guo Liu [a]
[a] School of Materials Science and Engineering , Harbin Institute of Technology , PO Box 433, Harbin 150001 , China
Accepted author version posted online: 22 May 2012.Published online: 13 Jun 2012.

To cite this article: Xue-Song Liang , Jia-Hu Ouyang & Zhan-Guo Liu (2012) Preparation of $BaCrO_4$ particles in the presence of EDTA from aqueous solutions, Journal of Coordination Chemistry, 65:14, 2432-2441, DOI: 10.1080/00958972.2012.696106

To link to this article: http://dx.doi.org/10.1080/00958972.2012.696106

Journal of Coordination Chemistry
Vol. 65, No. 14, 20 July 2012, 2432–2441

Taylor & Francis
Taylor & Francis Group

Preparation of $BaCrO_4$ particles in the presence of EDTA from aqueous solutions

XUE-SONG LIANG, JIA-HU OUYANG* and ZHAN-GUO LIU

School of Materials Science and Engineering, Harbin Institute of Technology, PO Box 433, Harbin 150001, China

(*Received 19 December 2011; in final form 9 April 2012*)

$BaCrO_4$ particles with well-defined morphologies have been synthesized in the presence of EDTA as a crystal growth modifier from aqueous solutions. The influence of pH on the morphology of $BaCrO_4$ crystals with and without EDTA additive was investigated to better understand the formation mechanism. EDTA has a strong interaction with the crystal faces of $BaCrO_4$ and influences the final morphology of $BaCrO_4$ crystals. In the presence of EDTA, $BaCrO_4$ particles at pH = 6 always exhibit a spindle-like morphology due to the large inhibition effect of EDTA on the $BaCrO_4$ crystallization. With decreasing pH, the particle morphology changes into a peanut-type at both pH = 5 and pH = 4 due to the relatively low inhibition and the following secondary heterogeneous nucleation and growth. The possible morphological evolution of $BaCrO_4$ particles is also proposed.

Keywords: $BaCrO_4$; EDTA; Nanostructured materials; Crystal growth; Aggregation

1. Introduction

Inorganic materials with specific size and controlled morphology have been widely used in fields as diverse as modern materials, catalysis, medicine, ceramics, pigments, cosmetics, etc. [1, 2]. Compared with size control, morphology control or morphogenesis is more demanding to achieve by chemical methods [3–5]. Many studies on synthesis of inorganic crystals with complex superstructures were reported. For example, sulfide and zeolites with different hierarchical architectures [6, 7], Bi_2WO_6 uniform hierarchical microspheres [8], urchin-like $CdWO_4$ microspheres [9], and flower-like $Sr_2Sb_2O_7$ and $Y_2(WO_4)$ [10, 11] were fabricated from low-dimensional nanobuilding blocks based on different driving mechanisms in solution. Hydrothermal synthesis is becoming important in most systems reported for the formation of superstructures in solution. Generally, the hydrothermal method requires operating temperature above 100°C and special equipment (e.g. Teflon-lined autoclave and pressure apparatus), which increases the production cost and leads to difficulty for scale-up production. Therefore, exploiting facile and low-cost routes for designing and large-scale

*Corresponding author. Email: ouyangjh@hit.edu.cn

ISSN 0095-8972 print/ISSN 1029-0389 online
http://dx.doi.org/10.1080/00958972.2012.696106

preparation of materials with controlled shapes at room temperature has been a hot research issue but still remains a great challenge to chemists and material scientists.

One of the most intensely examined systems is the ABO_4 class of oxometallates, where A and B are two different metals with oxidation states of +2 and +6, respectively [12, 13]. $BaCrO_4$, for instance, has been widely used as a model system for study of morphological control of inorganic minerals [14]. It can also be used as an oxidizing agent, a catalyst for enhancing vapor-phase oxidation reaction and high temperature solid lubricants [15, 16]. Many recent efforts have been directed toward synthesis of $BaCrO_4$ particles with different morphologies at room temperature. For example, some template synthesis routes, including hard, and soft template methods, were employed to synthesize $BaCrO_4$ superstructures. Dendritic superstructural and fractal crystals of $BaCrO_4$ were synthesized by vegetal bi-templates [17], and ordered $BaCrO_4$ nanostructures were accomplished using the cationic reverse micelle method [14, 18]. In addition to the template method, by using water soluble double-hydrophilic block copolymers (DHBCs) as crystal modifiers, $BaCrO_4$ nanofibers can be self-assembled into hierarchical superstructures [19]. EDTA, having four carboxylic groups and two lone pairs on two nitrogen atoms as binding sites, can coordinate with most metal ions to form relatively stable M-EDTA complexes. The presence of EDTA in the reaction system is helpful for formation of several materials with well-controlled morphologies [20, 21]. Herein, a new and facile strategy is reported for morphological control of $BaCrO_4$ using EDTA as crystal growth inhibitor and saturation controller. EDTA and Ba^{2+} form a 1:1 complex at pH = 9 which dissociates below pH = 9. Hence, supersaturation of the solution can be controlled by adjusting the pH. In addition, EDTA also acts as a very effective crystal growth modifier to direct the controlled synthesis of $BaCrO_4$ particles with well-defined morphologies. $BaCrO_4$ crystals with different morphologies can be easily fabricated in the EDTA stabilized solution by adjusting the pH. The key role of EDTA in fabrication of $BaCrO_4$ particles is also proposed.

2. Experimental procedure

As the solubility of $BaCrO_4$ in water is very small, Ba^{2+} and CrO_4^{2-} ions cannot be stabilized in the absence of a complexing agent. The disodium salt of EDTA was chosen for this purpose. $BaCl_2 \cdot 6H_2O$, Na_2CrO_4, and disodium salt of EDTA were supplied from Tianjin Bodi Chemical Reagent Corporation, China. All chemicals were of analytical grade and used without purification. In a typical synthesis procedure, 0.5 mmol $BaCl_2 \cdot 6H_2O$, 0.5 mmol Na_2CrO_4, and 2.5 mmol disodium salt of EDTA were dissolved in 50 mL distilled water in a glass beaker (final concentration 0.01 mol L^{-1} of $BaCrO_4$ and 0.05 mol L^{-1} of EDTA). The solution immediately becomes cloudy with yellow precipitates. When the pH was adjusted to 9 by adding NaOH, the solution becomes clear. The solution was kept under static condition in air for 24 h, and no chemical precipitation was observed. Then, the appropriate quantity of HCl solution was added into the pH-adjusted solution drop by drop under continuous stirring to decrease the pH. To investigate the influence of pH on the crystallographic morphology of products with EDTA additive, the final pH values of the reaction solutions were adjusted to 7, 6, 5, 4, and 3 by adding appropriate quantity of HCl solution. No

precipitation was observed in solutions with the pH values of 7 and 3, respectively, which remain unchanged after static observation even for 2 weeks. However, yellow precipitates were clearly observed in those solutions with the pH values of 4, 5, and 6 after induction time of 30–60 min. The suspension was kept at room temperature for 3 days and then precipitates were collected by centrifugation. Finally, $BaCrO_4$ products were obtained after drying the precipitates in air at 80°C for 12 h. As a comparative study, $BaCrO_4$ particles were also prepared without EDTA. Na_2CrO_4 solution was added quickly into aqueous solution of $BaCl_2$ under vigorous stirring at room temperature (the pH values of both solutions were adjusted to a certain value). After stirring for 30 min, the solution was kept for 3 days to obtain $BaCrO_4$ precipitates.

The phase structure of the products was identified by an X-ray diffractometer (XRD; Rigaku D/Max 2200VPC) using Cu-Kα radiation at a scan rate of $4^\circ\,min^{-1}$ in a 2θ range of 10–70°. The morphology of $BaCrO_4$ products was observed by a scanning electron microscope (SEM; FEI Quanta 200 F, the Netherlands) at an accelerating voltage of 20 kV. Equilibrium constant data used in this article were obtained from the on-line JESS thermodynamic database [22].

3. Results and discussion

By adding appropriate quantity of HCl solution drop by drop under continuous stirring, the final pH of the reaction solutions were adjusted to 7, 6, 5, 4, and 3. Yellow precipitates were obtained only in those solutions whose pH values were 6, 5, and 4. No chemical precipitation was observed in solutions with pH of 7 and 3, which remain unchanged for 2 weeks. Figure 1 shows the XRD patterns of the yellow products obtained at different pH values in the presence of EDTA. All the diffraction peaks can

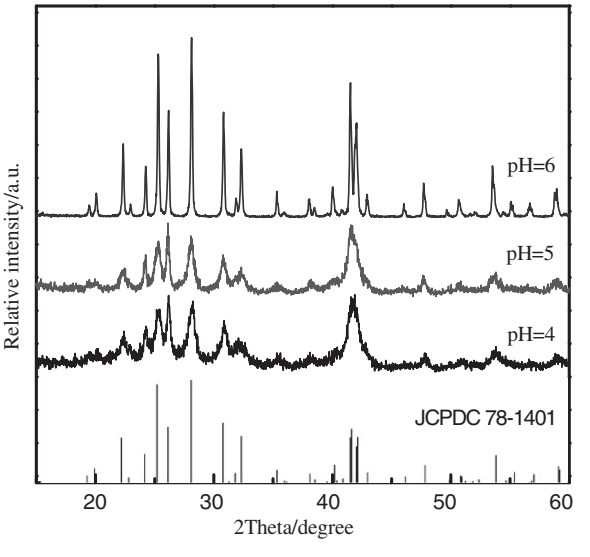

Figure 1. XRD patterns of the obtained yellow precipitates at different pH values in the presence of EDTA.

be perfectly indexed to the orthorhombic phase of $BaCrO_4$ (JCPDC 78–1401, with lattice parameters $a = 9.113$ Å, $b = 5.528$ Å, $c = 7.336$ Å). The width and intensity of the XRD peaks vary obviously with pH. The half-width of the XRD profiles of the $BaCrO_4$ particles synthesized at pH values of 4 and 5 broaden in comparison with the result obtained at pH = 6, proving that the $BaCrO_4$ particles synthesized at pH = 4 and pH = 5 are composed of very fine crystallites as subunits. The relative intensity of diffraction peaks for $BaCrO_4$ products obtained at pH = 6 are similar to the reported XRD data for $BaCrO_4$ in JCPDC 78–1401. However, the intensity ratios $I(210)/I(102)$ of diffraction peaks for the $BaCrO_4$ products synthesized at pH values of 4 and 5 are 0.92 and 0.89, respectively, much lower than the reported $I(210)/I(102)$ result of 1.76. This implies that the products synthesized at pH of 4 and 5 have a preferred growth direction, which may result in the occurrence of transition morphology of $BaCrO_4$ crystal.

The morphology of as-synthesized $BaCrO_4$ particles in the presence of EDTA additive is shown in figure 2. The low magnification SEM image in figure 2(a) clearly displays that well-defined, peanut-type particles with a mean length of 2.0 μm are synthesized at pH = 5. Figure 2(c) shows the morphology of $BaCrO_4$ particles obtained at pH = 4. The particles still have a peanut-type morphology but with two larger ends. The surfaces of the products synthesized at pH values of 4 and 5 are not smooth. The high magnification SEM images in figure 2(b) and (d) reveal that the relatively rough surfaces of the $BaCrO_4$ particles are composed of very fine crystals, which are responsible for the breadth of the XRD peaks. The mean sizes of these fine crystals are calculated by comparing the full width at half maximum of the most intense peak (102). The mean sizes of $BaCrO_4$ subunits are calculated to be 21 nm (pH = 5) and 28 nm (pH = 4) according to the Scherrer equation [23]. However, the $BaCrO_4$ product obtained at pH = 6 changes into a spindle-like morphology, as shown in figure 2(e).

The formation and morphological variation of $BaCrO_4$ shows a strong influence of pH value on nucleation and growth processes of crystals. The formation mechanism of $BaCrO_4$ particles is closely related to the coordination of Ba^{2+} and EDTA to form Ba-EDTA complex in the initial solutions, then the dissociation of the complex and the formation of $BaCrO_4$. The reactions in aqueous solutions are summarized in table 1.

Barium chloride and disodium EDTA react to yield $[Ba\text{-}EDTA]^{2-}$ and $[Ba\text{-}EDTA]^{-}$ in reactions 2 and 3. Since no solid-phase precipitation was observed at high pH values (such as pH = 7 or more) even after a long period, it is concluded that free Ba^{2+} ion concentration was not sufficiently high for achieving supersaturation and the barium complexes did not contribute to nucleating events of any solid phase. Reactions 4–7 in table 1 show that these complex formations depend on pH value. The protonation state of EDTA naturally depends on pH, and the conditional constant will vary with pH value. As the conditional constant of the Ba-EDTA complex mentioned is changed with pH, decreasing the pH of the solution promotes a low conditional constant, which will lead to dissociation of the complex and subsequent release of free barium ions. Thus, supersaturation of the solution becomes available for the nucleation and growth of $BaCrO_4$ crystals. The chromium(IV) ions are in equilibrium as indicated by equations (8) and (9) in water. It can be easily derived from the reaction equations that the concentration of CrO_4^{2-} will decrease with decreasing pH value. Thus, $BaCrO_4$ precipitate cannot be obtained at low pH values (such as pH = 3 or less).

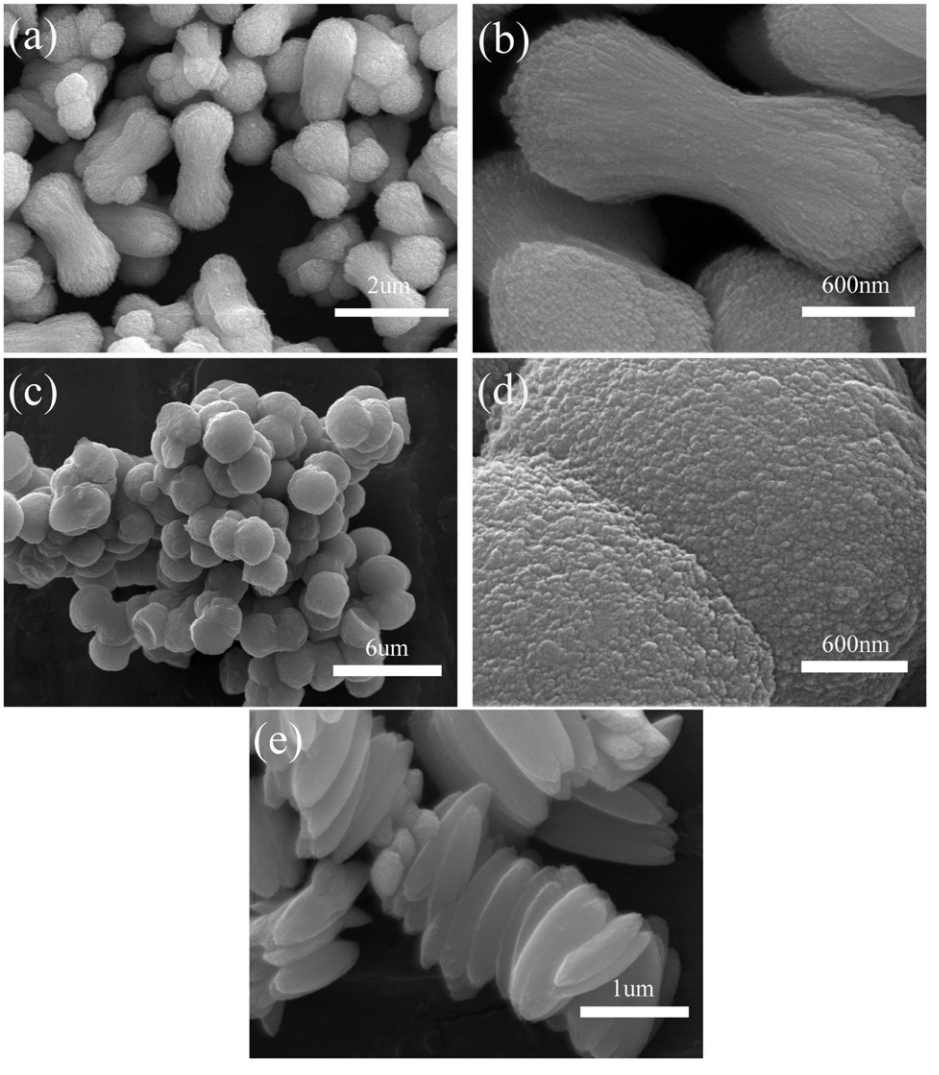

Figure 2. SEM images of $BaCrO_4$ particles in the presence of EDTA additive synthesized at different pH values: (a) and (b) pH = 5; (c) and (d) pH = 4; (e) pH = 6.

Table 1. The reactions and thermodynamic constants used to calculate the species distribution in aqueous solution.

Reaction	Equilibrium	log K
1	$Ba^{2+} + CrO_4^{2-} = BaCrO_4$	9.92
2	$Ba^{2+} + EDTA^{4-} = [BaEDTA]^{2-}$	9.336
3	$Ba^{2+} + EDTA^{4-} + H^+ = [BaHEDTA]^-$	14.6
4	$EDTA^{4-} + H^+ = HEDTA^{3-}$	10.61
5	$EDTA^{4-} + 2H^+ = H_2EDTA^{2-}$	17.68
6	$EDTA^{4-} + 3H^+ = H_3EDTA^-$	19.92
7	$EDTA^{4-} + 4H^+ = H_4EDTA$	23.19
8	$CrO_4^{2-} + H^+ = HCrO_4^-$	6.49
9	$2HCrO_4^- = CrO_7^{2-} + H_2O$	1.51

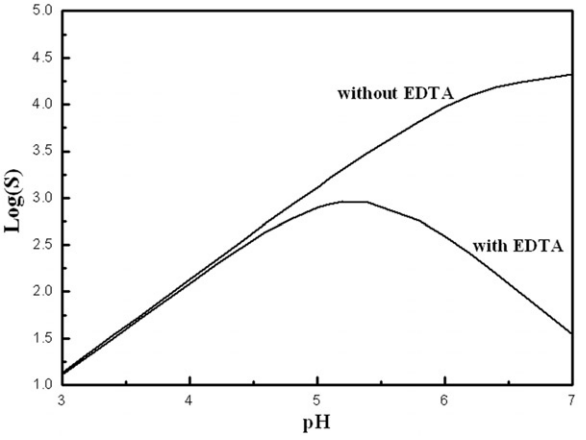

Figure 3. Supersaturation of $BaCrO_4$ as a function of pH with and without EDTA.

The influences of EDTA addition and pH value on crystal nucleation and growth are expressed in terms of the solution supersaturation (S). Supersaturation, the thermodynamic driving force for $BaCrO_4$ formation, can be defined as

$$S = \frac{\alpha(Ba^{2+})\alpha(CrO_4^{2-})}{K_{sp}},$$

where $\alpha(Ba^{2+})$ is the activity of Ba^{2+}, $\alpha(CrO_4^{2-})$ is the activity of CrO_4^{2-}, and K_{sp} is the solubility constant of $BaCrO_4$ at 25°C ($K_{sp} = 9.92$).

The initial supersaturation of experimental solutions, assuming ideally mixed reactor content and no precipitation, is calculated using PHREEQC – a software tool for geochemical calculations supplied by the US Department of the Interior. The code uses the classical theory of nucleation and growth to determine the chemical speciation of a solution [24]. On the basis of this speciation the supersaturation of a given salt is calculated. The equilibrium constants are taken mainly from the WATEQ database supplied with PHREEQC. However, the database was extended with data from other sources (see table 1).

The calculated supersaturation of $BaCrO_4$ at different pH values in the system is represented in figure 3. As seen, the log(S) curve obtained in the presence of EDTA is consistent with the experimental results. The supersaturation first increases and then decreases with decreasing pH, and reaches maximum at about pH = 5. An enhancement of metastable zone width with the addition of EDTA leads to inhibition of $BaCrO_4$ nucleation, while the supersaturation is still at a high level at pH = 3 and pH = 7 [25]. The induction time was determined through the change in the opacity of the solution. Although this method may have some errors, it can be used to compare the length of the induction time. According to classical nucleation theory, decrease in supersaturation should lead to a longer induction time [24]. However, when the final pH values of the reaction solutions were adjusted to 6, 5, and 4, respectively, the solution with a pH of 4 became turbid much earlier than those with pH of 5 and 6. The lowest supersaturation at pH = 4 leads to the shortest induction time. Obviously, the introduction of EDTA in the system leads to great change in the crystal nucleation process.

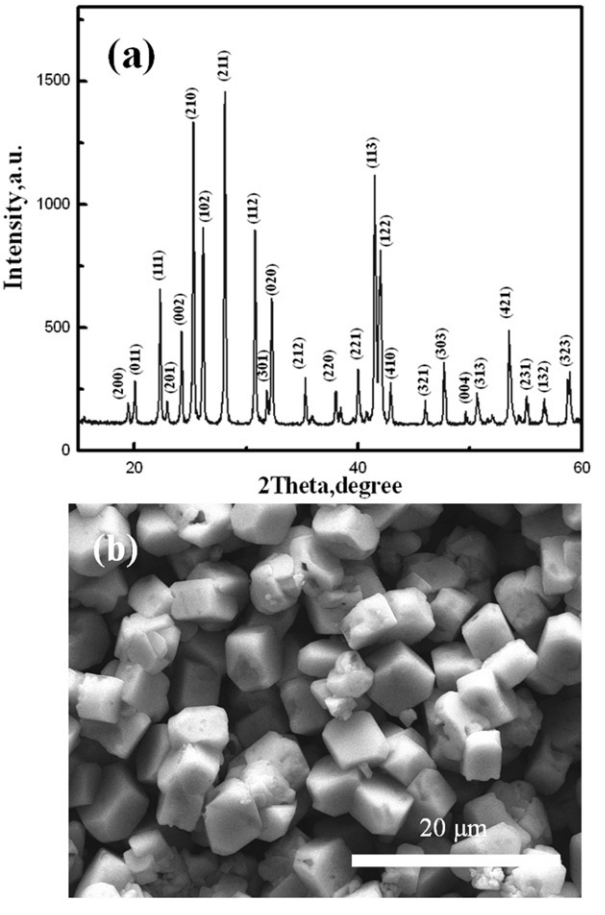

Figure 4. XRD pattern and SEM micrograph of $BaCrO_4$ particles synthesized without EDTA: (a) XRD pattern; and (b) SEM micrograph.

Another log(S) curve in figure 3 is obtained for the situation where EDTA is absent. Without EDTA additive, the supersaturation decreases with decreasing the pH and becomes closer to the curve obtained in the presence of EDTA additive at pH = 4. A comparative study was carried out at pH = 4 without EDTA additive to examine the role of EDTA. At a high supersaturation level, the solution without any inhibition becomes turbid as soon as Na_2CrO_4 was added to the system. Figure 4(a) shows the XRD pattern of the $BaCrO_4$ particles synthesized without EDTA additive. The sharp diffraction peaks of the samples indicate that the $BaCrO_4$ particles are well crystallized. The morphology of the as-synthesized $BaCrO_4$ particles in the absence of EDTA is shown in figure 4(b). No peanut-type or strip-like $BaCrO_4$ particles can be obtained under this condition. $BaCrO_4$ particles synthesized without EDTA additive exhibit well-crystallized crystals with a mean size of about 5 μm. At the same supersaturation level, the crystals are clearly large instead of nano-superstructures without well-crystallized faces. This result shows that EDTA has a strong interaction with the crystal faces of $BaCrO_4$, which can influence the final morphology of the crystal.

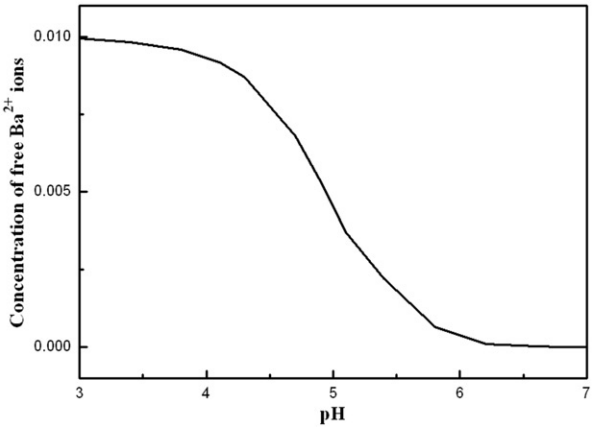

Figure 5. The concentration of free barium ions as a function of pH.

In a solution containing both EDTA and barium ions, the barium ions have three types: free barium ions and two types of EDTA complexes (see table 1). The concentration of free barium ions at different pH values can be calculated with PHREEQC. Figure 5 illustrates that the concentration of free barium ions decrease with increasing pH. Although this curve can only represent the initial situation of the solution, a trend that the binding interaction of EDTA on the $BaCrO_4$ crystals weakens with decreasing pH can be inferred. EDTA is a very effective inhibitor for crystallization due to the strong interaction between the EDTA and growing crystals, such as $BaSO_4$ or $CaCO_3$ [25, 26]. Thus, the inhibition for the crystallization increases with increasing pH.

On the basis of the above results, the growth behavior of $BaCrO_4$ crystals at different pH values has two types. The peanut-type particles with different sized ends were synthesized at a relatively low degree of inhibition for crystallization of $BaCrO_4$, while the spindle-like particles were synthesized at a relatively high degree of inhibition. In an ionic solution with concentrations far above the saturation level, amorphous clusters are formed first, which then produce the crystalline nuclei at a later stage [27, 28]. At higher inhibition, the secondary heterogeneous nucleation and growth are inhibited. Aggregation-mediated crystallization leads to formation of spindle-like $BaCrO_4$ particles. In the same way, monocrystalline ellipsoidal α-Fe_2O_3 can be synthesized by directional aggregation of small α-Fe_2O_3 ellipsoids [29]. At lower inhibition, the secondary heterogeneous nucleation and growth can occur and then influence the final morphology of the $BaCrO_4$ crystal. Sugimoto and co-workers [30–32] synthesized peanut-type hematite crystals with a very similar shape and size from a gel-sol method in the presence of sulfate. The adsorption of sulfate to the growing surfaces parallel to the *c*-axis resulted in the formation of hematite nanorods. The formation mechanism of the peanut-type shape was explained in terms of the gradual outward bending of dense rod-like subcrystals or nanorods on both ends of ellipsoidal particles by the growth of new crystalline nanorods in the space between the existing subcrystals. This growth process was strongly supported by computer simulation results [33]. In the present case, it is assumed that the EDTA plays a simple role on restricting crystallization of $BaCrO_4$. If there is a certain degree of nucleation on the side surfaces, the outward bending of

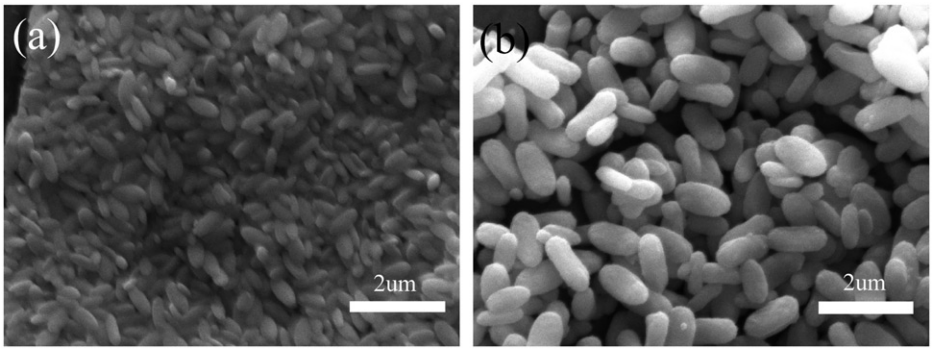

Figure 6. SEM images of $BaCrO_4$ particles obtained after aging for different time: (a) 30 min; and (b) 3 h.

subcrystals can be achieved, which can result in peanut-type particles. The nucleation probability on side surfaces would become larger if the binding interaction of EDTA on the side surfaces of $BaCrO_4$ nanocrystals becomes weaker. As the binding interaction of EDTA with $BaCrO_4$ decreases with decreasing pH, the nucleation probability on side surfaces would increase with decreasing pH, leading to the observed variation trend that the two ends of the peanut-type crystals become larger. From the XRD result, preferred crystal growth occurs in the crystallization process of the peanut-type $BaCrO_4$ particles. The faces with the largest growth rate will vanish in the final shape and exhibit relatively low diffraction intensity in the corresponding XRD pattern [34]. Upon surface cleavage of the (210) face of $BaCrO_4$ there are no Ba^{2+} ions on the surface open [19]. This suggests that EDTA does not favorably absorb on the (210) face, which may result in a fast growth rate while the other crystal faces are inhibited by the absorption of EDTA. Thus, a relatively low intensity of (210) peaks can be detected in the XRD patterns of the $BaCrO_4$ particles synthesized at both $pH = 4$ and $pH = 5$.

The $BaCrO_4$ products obtained at $pH = 4$ were analyzed after aging for different times to understand the growth mechanism of the peanut-type particles. Figure 6(a) represents a typical image of the product formed after 30 min and indicates the presence of small ellipsoidal particles with a mean size of about 600 nm. Figure 6(b) represents the $BaCrO_4$ product obtained after 3 h. Clearly, the increase in aging time from 30 min to 3 h induces growth of the $BaCrO_4$ particles, and the morphology changes from an ellipsoid-type to a near peanut-type. The aspect ratios of the particles obtained after aging for different times were also measured. The aspect ratios of the particles obtained after aging for 30 min and 3 h are 2.23 and 1.86, respectively, however, the aspect ratio of the particles obtained after aging for 3 days (figure 2c) is 1.46. The decrease in the aspect ratio with aging time illustrates a high growth rate on the side surface, which is consistent with the growth mechanism mentioned above.

4. Conclusions

EDTA is used as a very effective crystal growth modifier to direct the controlled synthesis of $BaCrO_4$ particles with well-defined morphologies. EDTA has a strong interaction with the crystal faces of $BaCrO_4$ and influence the final morphology of the

$BaCrO_4$ crystal. In the presence of EDTA, the obtained $BaCrO_4$ particles at pH = 6 always exhibit a spindle-like morphology due to large inhibition effect of EDTA on $BaCrO_4$ crystallization. With decreasing pH, the particle morphology changes into a peanut-type at both pH = 5 and pH = 4 due to the relatively low inhibition and secondary heterogeneous nucleation and growth. A possible morphological evolution mechanism for the formation of $BaCrO_4$ particles is proposed by accentuating the chelation and inhibition roles of EDTA.

Acknowledgments

The authors would like to thank financial support from the National 863 High-Tech Project (2006AA03Z537), the National Natural Science Foundation of China (NSFC-No. 50572020 and 51021002), and the Program for New Century Excellent Talents in University (NCET-06-0339).

References

[1] C. Burda, X.B. Chen, R. Narayanan, M.A. El-Sayed. *Chem. Rev.*, **105**, 1025 (2005).
[2] G.M. Whitesides. *Small*, **2**, 172 (2005).
[3] B. Judat, M. Kind. *J. Colloid Interface Sci.*, **269**, 341 (2004).
[4] G.J. de, A.A. Soler-Illia, C. Sanchez, B. Lebeau, J.N. Patarin. *Chem. Rev.*, **102**, 4093 (2002).
[5] H.M. Keizer, R.P. Sijbesma. *Chem. Soc. Rev.*, **34**, 226 (2005).
[6] Q.R. Zhao, Y. Xie, Z.G. Zhang, X. Bai. *Cryst. Growth Des.*, **7**, 153 (2007).
[7] L. Tosheva, V.P. Valtchev. *Chem. Mater.*, **17**, 2494 (2005).
[8] Y.Y. Li, J.P. Liu, X.T. Huang, G.Y. Li. *Cryst. Growth Des.*, **7**, 1350 (2007).
[9] Y.C. Ling, L. Zhou, L. Tan, Y.H. Wang, C.Z. Yu. *CrystEngComm*, **12**, 3019 (2010).
[10] H. Xue, Z.H. Li, H. Dong, L. Wu, X.X. Wang, X.Z. Fu. *Cryst. Growth Des.*, **8**, 4469 (2008).
[11] L. Xu, J.M. Shen, C.L. Lu, Y.P. Chen, W.H. Hou. *Cryst. Growth Des.*, **9**, 3129 (2009).
[12] S.H. Yu, M. Antonietti, H. Clfen, J. Hartmann. *Nano Lett.*, **3**, 379 (2003).
[13] M. Li, S. Mann. *Langmuir*, **16**, 708 (2000).
[14] H.T. Shi, L.M. Qi, J.M. Ma. *Adv. Mater.*, **15**, 1647 (2003).
[15] W.S. Wang, C.Y. Xu, L. Zhen. *Mater. Lett.*, **61**, 3146 (2007).
[16] J.H. Ouyang, S. Sasaki, K. Umeda. *Surf. Coat. Technol.*, **154**, 131 (2002).
[17] Y. Yan, Q.S. Wu, L. Li. *Cryst. Growth Des.*, **6**, 769 (2006).
[18] Z.G. Li, J.L. Zhang, J.M. Du, B.X. Han. *Mater. Chem. Phys.*, **91**, 40 (2005).
[19] S.H. Yu, H. Clfen, M. Antonietti. *Adv. Mater.*, **15**, 133 (2003).
[20] H. Deng, C.M. Liu, S.H. Yang, S. Xiao, Q.Q. Wang. *Cryst. Growth Des.*, **8**, 4432 (2008).
[21] H.W. Zhang, X. Zhang, H.Y. Li, Z.K. Qu, S. Fan. *Cryst. Growth Des.*, **7**, 820 (2007).
[22] P. May, K. Murray, http://jess.murdoch.edu.au/jess/jess_home.htm
[23] K. Mogyorosi, I. Dekany, J.H. Fendler. *Langmuir*, **19**, 2938 (2003).
[24] N.P. Rajesh, K. Meera, C.K.L. Perumal, P.S. Raghavan, P. Ramasamy. *Mater. Chem. Phys.*, **71**, 299 (2001).
[25] K.J. Westin, A.C. Rasmuson. *J. Colloid Interface Sci.*, **282**, 370 (2005).
[26] F. Jones, P. Jones, M.I. Ogden, W.R. Richmond, A.L. Rohl, M. Saunders. *J. Colloid Interface Sci.*, **316**, 553 (2007).
[27] J. Rieger. *Tenside Surfactants Deterg.*, **39**, 221 (2002).
[28] J. Rieger, E.H. Dicke, I.U. Rau, D. Boeckh. *Tenside Surfactants Deterg.*, **34**, 430 (1997).
[29] M. Ocana, M.P. Morales, C.J. Serna. *J. Colloid Interface Sci.*, **71**, 851 (1995).
[30] T.M. Sugimoto, M. Khan, A. Muramatsu, H. Itoh. *Colloids Surf. A*, **19**, 233 (1993).
[31] T.M. Sugimoto, M. Khan, A. Muramatsu. *Colloids Surf. A*, **70**, 167 (1993).
[32] D. Shindo, G.-S. Park, Y. Waseda, T. Sugimoto. *J. Colloid Interface Sci.*, **168**, 478 (1994).
[33] N. Sasaki, Y. Murakami, D. Shindo, T. Sugimoto. *J. Colloid Interface Sci.*, **213**, 121 (1999).
[34] X.Y. Meng, G.H. Tian, Y.J. Chen, Y. Qu, J. Zhou, K. Pan, W. Zhou. *RSC Adv.*, **2**, 2875 (2012).